Appl Phys B (2009) 97: 85–94
DOI 10.1007/s00340-009-3577-x

Applied Physics B
Lasers and Optics

Gain versus tuning issues to Q-switch with Yb^{3+}:LSO and amplify broad-bandwidth pulses

A. Jolly · G. Bourdet · H. Coic · J. Luce

Received: 15 January 2009 / Revised version: 14 April 2009 / Published online: 16 May 2009

Abstract The capability of a thin slab of Yb^{3+}:LSO to be tuned within a Q-switched cavity is demonstrated in a range of laser wavelengths from 1052 to 1065 nm. Using a side-pump architecture, to create a linear gain-stripe in the crystal of which the dimensions can be finely controlled, we generate 50 to 150 ns-wide pulses in the range 1–5 mJ. These experimental data are fitted with the theoretical predictions by means of comprehensive modeling. Our model involves all the relevant parameters for the discussion of energetic, spectral and spatial issues of interest to evaluate the potential of this quasi-three-level material in the field of broadband regenerative amplification. Thanks to pure homogeneous broadening, this finally helps us to size a consistent pump design dedicated to the amplification of broad-bandwidth pulses up to a few milli-joules near 1053–1056 nm, the range of wavelengths involved in *ICF*.

PACS 42.60.Fc · 42.60.Gd · 42.55.Xi · 42.55.Rz

1 Introduction to Yb^{3+}:LSO and the issue of broadband amplification

The field of the short-pulse sources to be coupled with high-energy lasers, such as those dedicated to the search of Inertial Confinement Fusion (*ICF*), has lead a number of developments regarding the pre-amplification of broad-bandwidth nanosecond-wide pulses [1, 2]. The involved range of wavelengths and energies are 1053–1056 nm and a few millijoules. Most of these sources make use of laser configurations referred to as Optical Parametric Chirped Pulse Amplification (*OPCPA*). The *OPCPA* technique makes possible efficient optical performance, but it suffers from complexity. Direct pre-amplification with the help of broadband regenerative amplifiers, using ytterbium-doped materials, could be another option in the search of more robust and less expensive architectures. Among the large variety of existing materials, Yb^{3+}:Lu_2SiO_5 (*LSO*) [3] has been identified as one of the most promising crystals. *LSO* benefits from relatively large emission cross-sections [4, 5] in the vicinity of 1053–1056 nm, in relationship with intrinsic broadband capabilities. Furthermore, the thermal conductivity, $K_{\mathrm{LSO}} = 5.3\ \mathrm{Wm^{-1}\,K^{-1}}$, lies in the same range of values as that of Yb^{3+}:YAG, $K_{\mathrm{YAG}} = 6.5\ \mathrm{Wm^{-1}\,K^{-1}}$, and it is less sensitive to the increase of doping levels. To our knowledge, nowadays, *LSO* and other ortho-silicate materials [6] have essentially been considered in Continuous-Wave pumping (*CW*) and *CW* laser action [7, 8], or *CW* mode-locking to generate low-energy ultra-short pulses [9]. Beyond *CW* pumping and the related laser operations, Quasi-Continuous Wave (*QCW*) pumping and low duty-cycle amplification may also help to produce more energetic pulses. Then, *QCW* operations may take advantage of higher available pump-powers and energy-storage capabilities in the material, to build high-gain regenerative amplifiers. A number of broadband regenerative amplifiers involving ytterbium-doped materials have already been demonstrated. References of interest can be found with Yb^{3+}:YAG [10, 11], Yb^{3+}:YLF [12], Yb^{3+}:glass [13, 14], Yb^{3+}:SYS [15], Yb^{3+}:KYW [16], Yb^{3+}:GYSO [17] or with Yb^{3+}:CaF_2 [18]. But the emission cross-sections of these materials near 1053–1056 nm

A. Jolly (✉) · H. Coic · J. Luce
CEA, Centre d'Etudes Scientifiques et Techniques d'Aquitaine, Chemin des Sablières, 33114 Le Barp, BP2, France
e-mail: alain.jolly@cea.fr

G. Bourdet
Ecole Polytechnique, CNRS, CEA, UPMC, Route de Saclay, 91128 Palaiseau, France

remain lower than that of *LSO* by a factor of 5 to 10. Considering the potential of the crystal despite the specific wavelength requirements for *ICF*, it is remarkable that no significant work has been published yet with *LSO*. The first step prior to a complete demonstration of broadband amplification, which could be based on the use of the configuration referred to as Chirped Pulse Amplification (*CPA*), of which the implementation is still beyond the scope of this paper, consists of Q-switching. Combining Q-switching and wavelength-tuning, we can benefit from any of the required conditions to evaluate the full broadband amplification capabilities of the material, up to the saturation of the gain. The aim of our paper is to relate the experimental results to proper modeling, versus the spectroscopic data, making possible sizing any single pulse amplifier. From the viewpoint of basic physics, thanks to pure homogeneous broadening effects in Yb^{3+}:LSO, broadband regenerative amplification can be directly tied to wavelength-tuning. So, this work aims to demonstrate the capability of the material to produce nanosecond pulses with millijoule energies in the 1050–1065 nm wavelength range, while considering spectral bandwidth of 10 nm or more pulses, exploring a consistent tuning range.

In the first step, we remember the expressions of the measurable parameters to characterize a given pulse from basic Q-switching, taking advantage of the analogy between the processes of Q-switching and of regenerative amplification. This is done by integrating the standard rate equations related to quasi-three-level materials and the role of each of the involved data can be clearly identified during the sequence of pulse build-up. This leads to fairly simple relationships for relating the theoretical and measurable parameters of the output pulse from a regenerative cavity. In the second step, we implement more comprehensive broadband modeling, using the complete spatial, spectral and temporal data from the cavity in connection with the spectroscopic data of the material. Our purpose consists of the prediction of the theoretical performance to be expected from a given laser configuration, i.e., the pump geometry and the architecture of the amplifier or Q-switched cavity. A number of modeling results will be provided for a large range of laser wavelengths. The presentation of the experimental setup for Q-switching then consists of the third step, together with measurement results. We use of a very simple grating-based multi-mode cavity design and Q-switching is experienced in combination with wavelength-tuning. The pulse repetition frequency is 1 Hz for avoiding thermal effects in the material. Our side-pump configuration involves a unique high-power diode-stack and a thin slab of Yb^{3+}:LSO. In the last step, we discuss the consistency of theoretical predictions and experimental data for fitting the results within the attainable range of wavelengths. The validation of the model also helps us to explore a few possible directions for the optimization of the pump design, versus actual sizing limitations.

2 Involved parameters and performance modeling

Let us consider the saturated amplification for the generation of millijoule pulses, in combination with up to 10 nm-wide optical bandwidths. The most easy-to-implement regenerative configuration to generate nanosecond-wide pulses consists of Q-switching. As compared with a true regenerative amplifier, the main limitation of a Q-switched cavity consists of the lack of any independent control, regarding the starting sequence from the Amplified Spontaneous Emission *(ASE)*-induced noise. In other respects, Q-switching will provide all the essential experimental data to verify and discuss the expected laser performance of the material. This is right for energy-storage, gain saturation and broadband amplification if the laser wavelength can be tuned at discretion. Two primary sizing data must be considered: the pumping rate (k), as the ratio of the actual pump power to the threshold pump power (P_{pump}), and the saturation energy density ($P_{\text{pump\_th}}$) of the material near the peak emission wavelength. The saturation fluence is $F_{\text{sat}} = \frac{hc}{\lambda\sigma_{\text{eL}}}$, where h and c are the *Planck* constant and the light velocity, λ is the wavelength and σ_{eL} is the emission cross-section. Then, for Yb^{3+}:LSO, $F_{\text{sat}} = 23\ \text{J cm}^{-2}$ at $\lambda \sim 1060$ nm. The processes of Q-switching and regenerative amplification can be described a simple way versus k with the help of a few basic relationships, which involve the value of peak output energy to be extracted [11] and the corresponding build-up time of the pulse. The amount of available output energy depends upon k and three other specific parameters, as determined by the quasi-three-level nature of the material and the cavity:

$$E_{\text{out}} = \frac{l_{\text{stripe}}}{L}[1-\beta][1+\xi]\gamma S_{\text{beam}} F_{\text{sat}} \times \left\{k - 1 - \frac{\ln[(1+\xi)k - \xi]}{1+\xi}\right\} \quad (1)$$

where S_{beam} is the beam cross-section, l_{strip} and L are the active material and the cavity lengths, respectively, $\beta = \frac{\sigma_{\text{aL}}}{\sigma_{\text{eL}}}$ is the ratio of the absorption and emission cross-sections at the laser wavelength. $\xi = 2\sigma_{\text{aL}} N_{\text{tot}} \frac{L}{\gamma_{\text{opt}}}$ is the ratio of the re-absorption losses inside the material itself to the optical losses in the cavity, γ_{opt}. The principle of the calculations leading to (1) involves a set of simplified rate equations, using a basic representation of the material by means of a quasi-three-level energy diagram. The derivation of the output energy at the peak of the so-called Q-switched envelope helps to account for the saturation of the gain resulting from

regenerative amplification and the definitions of k and F_{sat}. The energy transfer characteristic of a Q-switched laser design can be determined by a simple way from (1) by ranging k, assuming a simple determination of ξ and β from the spectroscopic data at the peak laser wavelength λ. Two additional equations can also be used to depict the build-up time of the related pulse and the small-signal gain. The build-up time will consist of an easy-to-measure data, for the evaluation of the performance given a particular regenerative amplifier or Q-switched cavity. The number (N) of round-trips within the amplifying cavity is connected to the build-up time by $T_c = 2N\frac{L}{c}$, where

$$T_c = \frac{4L}{c(\gamma + 2\sigma_{\text{aL}} N_{\text{tot}} l_{\text{stripe}})(k-1)} \ln\left(\frac{F_{\text{sat}}}{F_{\text{ASE}}}\right), \tag{2}$$

$$G_o = \exp\left\{\left[\frac{(\sigma_{\text{eL}} + \sigma_{\text{aL}}) P_{\text{pump\_abs}} T_{\text{pump}}}{h\nu_{\text{pump}} V_{\text{pump}}} - \sigma_{\text{aL}} N_{\text{tot}}\right] l_{\text{stripe}}\right\}. \tag{3}$$

In (2), $\gamma = \ln(\frac{1}{R_{\text{coupler}}}) + \gamma_{\text{opt}}$ figures in the total optical losses inside the cavity, as a result of output coupling and internal optical absorption in excess of the re-absorption from the material. F_{ASE} is the starting spectral-noise intensity due to the fraction of contributing *ASE* contained within the mode volume of the cavity, and k is the mean inversion ratio over the lasing threshold.

In (3), $h\nu_{\text{pump}}$, T_{pump}, $P_{\text{pump\_abs}}$, V_{pump}, and N_{tot} are the pump photon energy, the pump pulse duration and the absorbed peak power from the pump, the pump volume and the doping level. The actual value of F_{ASE} within the complete amplification bandwidth ($\Delta\nu = 100$ nm) can be estimated using the product of the basic photon energy contained within a given mode cavity ($h\nu\Delta\nu$) by the total number of modes (M) oscillating in the cavity. Representative conditions related to our forthcoming experiments imply $M \sim 30$ to 50 modes. The spatial overlap between the pump and the amplifying cross-sections ranges from 40 to 60%, the value of F_{ASE} within the complete spectral bandwidth of interest is on the order of 2 to 4 mW cm^{-2}. The pump power at the threshold is governed by the optical losses and by the transparency threshold of the material, according to the following expression:

$$P_{\text{pump\_th}} = \frac{V_{\text{pump}} h\nu_{\text{pump}}}{T_{\text{pump}}\eta_{\text{transfer}}} \frac{\gamma + 2\sigma_{\text{aL}} N_{\text{tot}} l_{\text{stripe}}}{2(\sigma_{\text{eL}} + \sigma_{\text{aL}}) l_{\text{stripe}}}, \tag{4}$$

where η_{transfer} is the pump transfer efficiency from the stack to the gain-stripe. Regarding the effectiveness of (1)–(4) in the comparison of the measured and the estimated values of output-energy and build-up time, we essentially need to put numbers on the spatial overlap between the mode volume of the cavity, and on the proper theoretical amount of *ASE*. Regarding the basics of gain tuning, (2) also helps to remember that Q-switching remains a worst case when compared to the process of regenerative amplification. Actually, the build-up time of the Q-switched pulse is governed by the integrated spectral density of *ASE* power contained within the spectral bandwidth of the cavity. This implies that the process of amplification starts from quite a low value of input energy.

The spectral variations experienced by the emission cross-section of Yb^{3+}:LSO, which is denoted by $\sigma_e(\lambda)$, have been computed using the measured absorption and fluorescence spectra. The computations are based on reciprocity methods, and *Futchbauer–Ladenburg* procedures towards the longer wavelengths. The variations in the measured absorption and emission cross-sections [11], $\sigma_e(\lambda)$ and $\sigma_a(\lambda)$, are given in Fig. 1, along the three axes of the crystal. They reveal a large anisotropy. Starting from $\lambda = 1060$ nm, the location of the most efficient laser wavelength in the range of interest for amplification, the quasi-three-level scheme tends to match a nearly four-level scheme towards the longer wavelengths. Accounting for the re-absorption effects, the most efficient tuning range to be expected then ranges from 1050 to 1080 nm, typically. It can also be seen that the unique polarization of interest lies in the plane of the X axis.

In Fig. 2, we present the evolution of the spectral cross section versus the inversion ratio, following the X polarization. A very broad emission bandwidth is evidenced, which is consistent with the demonstration of pulses as short as 120 fs by mode-locking [19]. The zero line at 978 nm exhibits the larger absorption cross-section ($\sigma_{\text{aP}} = 4.76$ cm^2). Nevertheless, as the lower sublevel of the excited state is thermally populated, the inversion rate accessible is low compared to the one for shorter pump wavelengths. Then we use a pump wavelength and a pump pulse duration of 935 nm and 1 ms, respectively. As indicated in the bottom section of Fig. 1, a good approximation of $\sigma_e(\lambda)$ is given by:

$$\sigma_e(\lambda) = \sigma_o \exp\left[-\frac{(\lambda - \lambda_o)^2}{\Delta\lambda_o^2}\right] \sum_{i=1}^{10} \frac{k_i}{1 + (\frac{\lambda - \lambda_i}{\Delta\lambda_i})^2}. \tag{5}$$

The numerical values of λ_o and $\Delta\lambda_o$ are 1000 nm and 100 nm, while those of the different λ_i, their related linewidths $\Delta\lambda_i$ and intensities k_i are specified in Table 1. The different *Lorentzian* envelopes help us to match the different sites in the energy distribution of ytterbium. In (5), $\sigma_o = 1.1 \times 10^{-20}$ cm^2.

In the vicinity of $\lambda = 1060$ nm, (1)–(4) provide relevant orders of magnitude and help us relate the variations in the Q-switched or amplified pulse a simple way to measurable parameters. But the accurate description of competing broadband amplification and re-absorption effects, inside the material itself, needs to be verified using more comprehensive modeling with the help of more complex numerical tools. By means of high resolution sampling, both in

Table 1 The wavelength λ_i, their related line-widths $\Delta\lambda_i$ and intensities k_i for the analytical fit of (5)

Wavelength (nm)	978.6	991.5	993	1002	1010.5	1020	1032.5	1043.4	1057	1084
Line width (nm)	3.4	3.8	20	7	7	7	8	5	8	7
Coefficient k_i	0.52	0.37	0.2	0.35	0.2	0.15	0.58	0.38	0.97	0.55

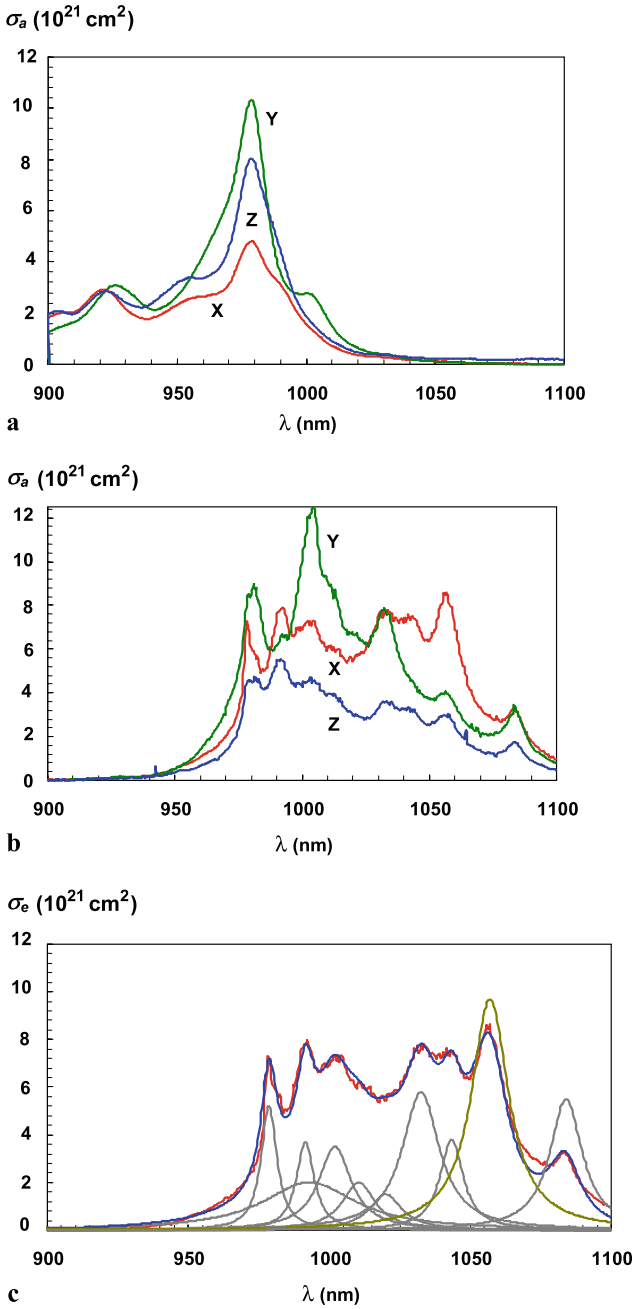

Fig. 1 Absorption (**a**) and emission (**b**) cross-sections for the three optical axis of Yb^{3+}:LSO and analytical fit of the emission cross-section following the X axis (**c**) to implement numerical calculations

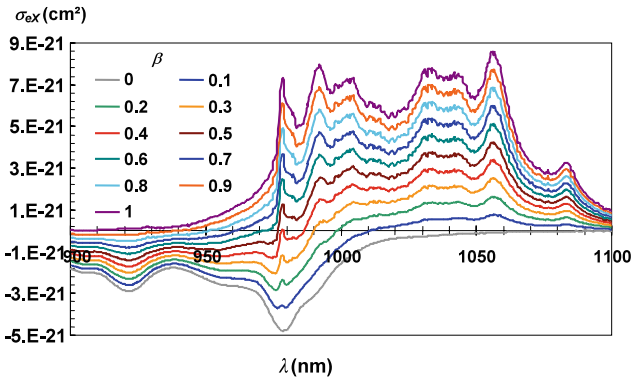

Fig. 2 Evolution of the spectral cross section versus the inversion ratio

the spatial and the spectral domains while accounting for a precise description of the pump geometry, we attempt to develop the calculations within the overall range of laser wavelengths involved in Figs. 1 and 2. As a matter of fact, due to the very small gain values, one can expect from the small values of $\sigma_e(\lambda)$, the actual pump geometry and the spatial overlap with the modal volume will consist of critical issues. They need to be addressed with the tight precision, to be confident with the computed evolutions of the linear and of the saturated gain distributions inside the active area of the slab. We implement the dedicated model in *MIRO*, a widely used numerical propagation code [20] which is used for beam propagation within high-energy laser architectures. *MIRO* also accounts for quasi-three-level systems. In particular, the related re-absorption effects can be considered together with broadband spectral amplification. The complete rate equations are solved numerically, starting from the treatment of each contributing laser transition across the involved multiplets in the energy diagram of the material. The temporal and spectral scales involved during the computations are sampled with the help of self-adaptive sizing windows. Successive temporal slices propagate along the slab of Yb^{3+}:LSO to provide a consistent description of the evolution of the instantaneous laser field inside the material itself, in such a way that the spatial distribution of the actual remaining energy after amplification in the slice $\#N$ defines the input spatial distribution of the gain to be available for slice $\#N + 1$. The sequential passes during the process of regenerative amplification are cascaded the same way. Then, we can monitor the gain-narrowing effects step by step in the presence of gain saturation, at the time of occurrence of each amplification pass. True homogeneous

broadening is assumed in the crystal, throughout the whole 100 nm-wide spectral fluorescence-bandwidth. Since the numerical process consists of a pure propagating sequence, local saturation effects due to spatial hole-burning cannot be considered. Thanks to the mirror–slab spacing and highly multi-mode operation, this will not be a problem. Furthermore, referring to physical limitations in our model, the thermo-optical and thermal lens effects are put apart. But the curvature radius of the rear reflector in the optical scheme is selected in such a way that the stability domains of the experimental set-up and of the figured cavity are about the same. This means that both modal volumes are also about the same, which will help to validate the comparison of the calculated and the measured values of output energy.

Let us now get back to the Q-switching process itself. We suppose that amplification is arbitrarily initiated from a short temporal spike at a given energy and a given wavelength. The spectral density in energy—or in peak power—of the initial spike is described using (5). The wavelength-normalization is made at the location of the peak $\sigma_e(\lambda)$, $\lambda = 1060$ nm. Provided a given λ, the energy of the spike determines the build-up time to reach the saturation of the gain. Regarding the neighboring wavelengths, the build-up time will experience plus or minus large variations as a function of the variations in $\sigma_e(\lambda)$. Since Q-switching actually starts from the fractional part of *ASE* contained within the mode volume and within the spectral bandwidth of the cavity, as already underlined, we do not care for exact initial conditions: The *ASE* rather looks like a continuous emission. However, thanks to the selection of a spike of which the duration is shorter than the round-trip time, there will not be any significant change in the computational results of the spectral gain saturation features. Besides the temporal issues, we account for the actual distribution of optical losses. We make use of a single *Pockels* cell, a polarizer and a variable output coupling. The cavity length is $L = 15$ cm. Considering a cavity length and an active cross-section of the gain-stripe of 3 mm and 3 mm^2, respectively, a number of modeling results are given in Fig. 3. When the integrated value of the small-signal gain (G_o) throughout the gain-stripe is raised from 1.15 to 1.3 (top section), given total optical losses $\gamma = 10\%$, the expected tuning range enlarges from 1055–1065 nm to 1050–1070 nm. The intracavity energy undergoes variations from 5 to 40 mJ, which corresponds to output energies comprised between ~0.5 and nearly 5 mJ. The related build-up times and pulse widths (Fig. 3(c)) vary, respectively, from 1 to 2 µs and 20 to 200 ns *FWHM*.

All these numbers have to be considered as expected orders of magnitude, which now need to be compared with actual experimental data.

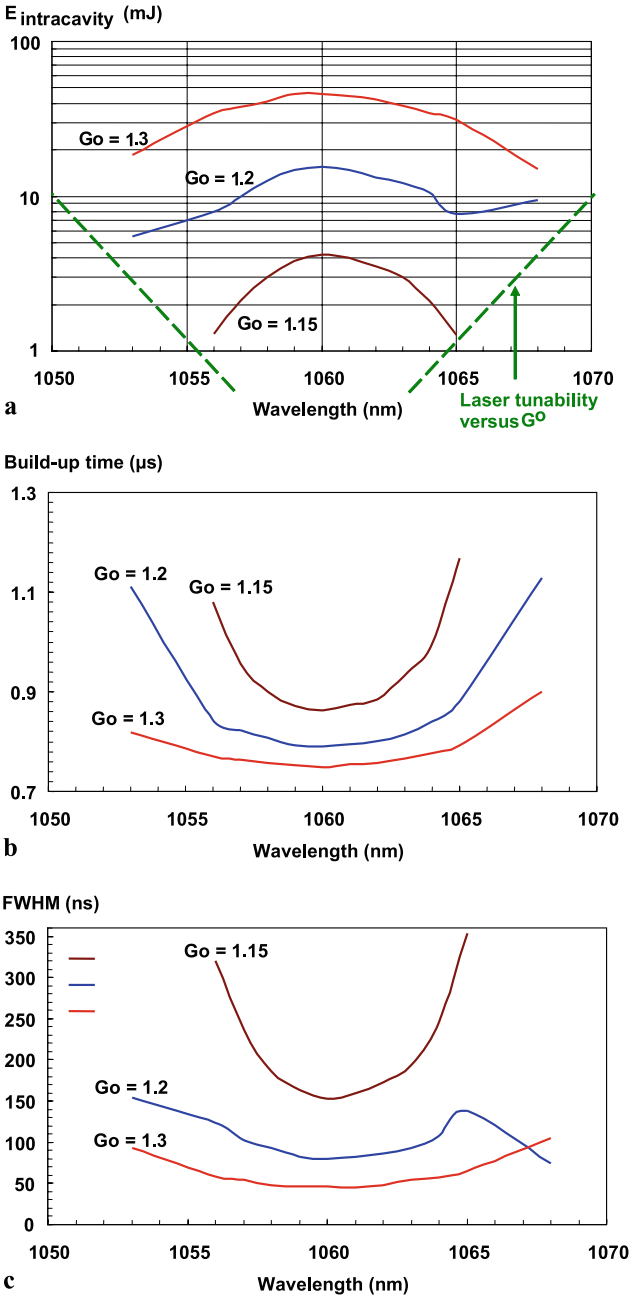

Fig. 3 Modeling the evolution of the Q-Switched energy, build-up time and pulse length versus selected wavelength inside the cavity. Cavity length = 15 cm, width of the pump area = 1.8 mm, internal losses = 10% and output mirror reflectivity = 90%

3 Tuning set-up for Q-switching experiments

Our Q-switched cavity uses a thin side-pumped slab [21] which is pumped with an unique *QCW* stack of 25 micro-lens-collimated diode-bars (Fig. 4(a)). The total emitting area and peak pump power equal 50 × 12 mm^2 and up to 2 kW during 1 ms. The diode-stack is focused onto the slab using three anti-reflection coated cylindrical lenses. This set of large aperture optics ensures the availability of quite in-

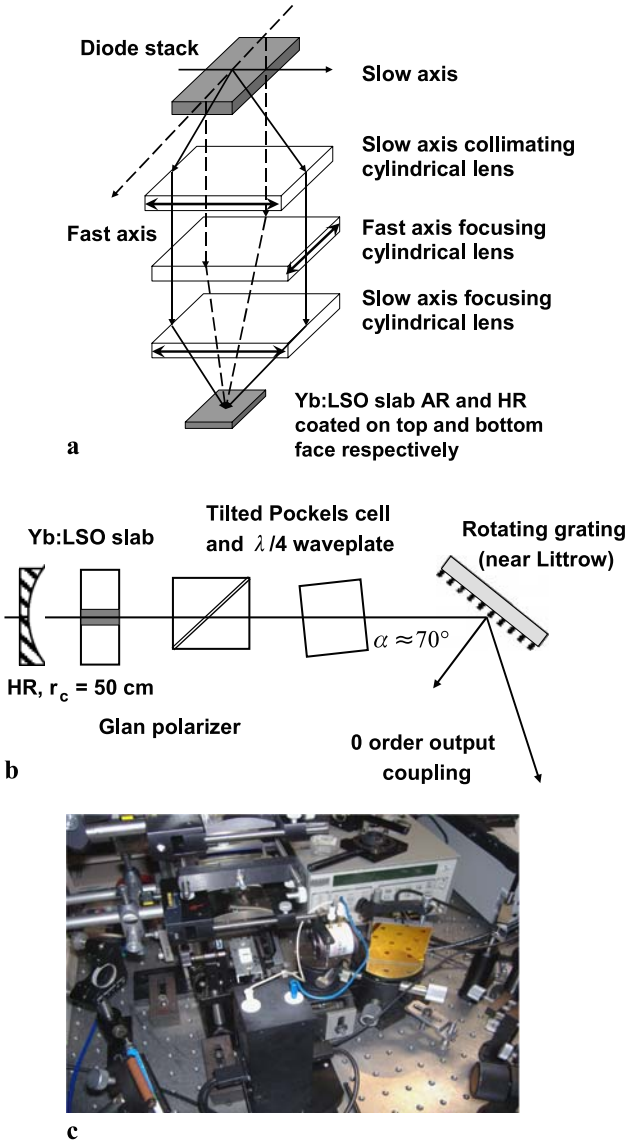

Fig. 4 Pumping scheme (**a**), optical set-up for tunable Q-switching (**b**) and the experimental implementation (**c**)

tense pump intensities in the central plane of the slab. The slab is 2 mm in thickness, 5 mm in width and 10 mm in length. The X axis of the crystal is parallel to the largest horizontal plane and normal to the beam path. The doping concentration is 10 at.%. Changing the position of one or two of the slow-axis cylindrical lenses, we can adjust the length of the gain-stripe while keeping a constant gain section. Moving the unique fast-axis cylindrical lens, we can adjust the amplifying section while keeping the length of the gain-stripe constant. The minimum size of the pump area in the plane of the slab can be made as small as 2.5×1 mm^2, which settles the highest pumping rate within the minimum volume of material, i.e., $V \approx 5$ mm^3.

Figure 5 shows the actual gain-stripe and the corresponding fluorescence distribution from the top of the pumped

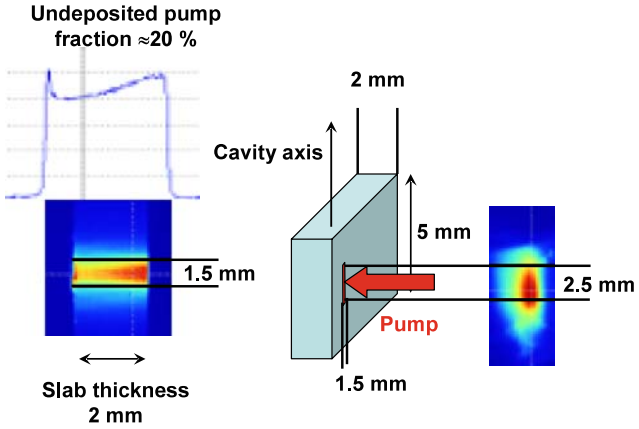

Fig. 5 Control of the gain geometry: near-field gain cross-section (*left*) and pump area from the top of the slab (*right*)

area, in the example of dimensions $\sim 1.4 \times 2$ mm^2. The pump energy density is up to 20–30 J cm^{-2}, under the strongest focusing conditions. These numbers are consistent with the search of the gain values specified above while accounting for relevant limitations, due to optical damage in the coatings which have been deposited on the faces of the slab. The top face is anti-refection coated and the bottom one is high-reflection coated. The most deleterious optical damage effects, to be prevented, are supposed to initiate from some uncontrolled high intensity spots within the pump area. Indeed, we do not use of any intermediate homogenizing optics. This is the reason for which peak pump fluence of 30 J cm^{-2} has been considered and that limits small-signal gain at around 1.3. The photograph in the left side of the figure evidences some amount of diffusion across the slab, apart from the pumped area, which materializes the un-pumped areas of the slab. Because of the rather low attainable values of the small-signal gain in Yb^{3+}:LSO, we have to minimize the optical losses anywhere, still preserving full tuning capabilities. To meet this requirement, we use of a rotating grating as the output coupler. The grating is operated near the *Littrow* incidence and that the reflection in the order $-1R$ ensures a large amount of internal feed-back, about 96%. The grating reflectivity does not vary by more than a fraction of 1% when the grating is rotated by up to about 10 degrees, which is enough to scan the entire bandwidth of interest. This way, we benefit from a well-defined, low-loss wavelength-selective output coupler of which the spectral transmission is determined by the coupling efficiency in the order 0. To get free from any parasitic spectral limitation, we include the necessary quarter-wave function inside the *Pockels* cell itself.

The cell only has to be tilted from its normal position by the required amount. Then the unique additional component to Q-switch the cavity is a *Glan* polarizer with broadband anti-refection coatings.

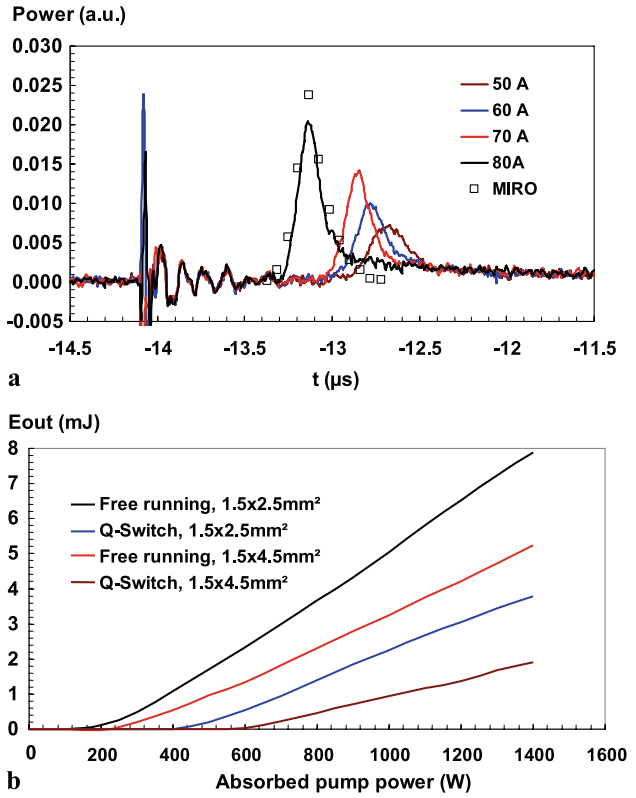

Fig. 6 Measured data when Q-Switching at 1059 nm with a gain stripe of which the dimensions are 1.5×2.5 mm^2, with standard coupler of which the reflectivity is 98% (**a**) and variations in the energy-transfer characteristic versus the pumping geometry (**b**). The superimposed dots in (**a**) show theoretical values from MIRO

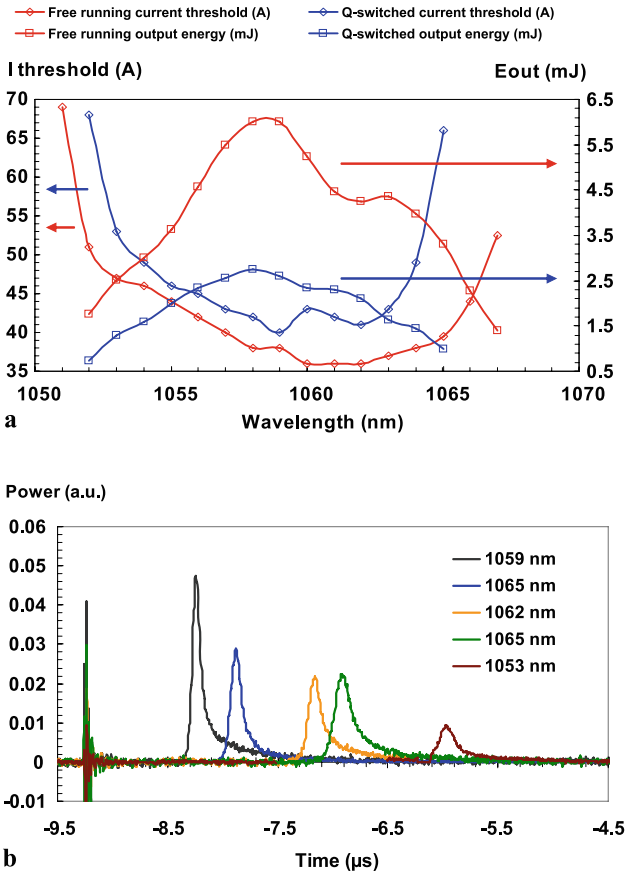

Fig. 7 Experienced tuning effects with the grating-based cavity, regarding the current threshold and output energy at constant pump power (**a**), and the variations in the Q-switched pulses (**b**)

Figures 6 and 7 provide a number of experimental results under different operating conditions. The evolution of the Q-switched pulse has been plotted. The emitted pulse shapes at 1060 nm for various pump intensities are shown in Fig. 6(a). For this experiment, the coupler is a standard mirror with broadband reflectivity and $R = 98\%$. The effective build-up time has been referred to the time of occurrence of the high-voltage transient on the left side of the curve. Increasing the peak pump power from 0.8 up to nearly 2 kW, the build-up time and the pulse-width *FWHM* decreases from 1.3 µs and 500 ns down to about 700 and 130 ns, respectively. Figure 6(b) presents the variation of the energy-transfer laser characteristic versus the pumping geometry. Under the condition of minimum optical losses, this first Q-switched configuration has produced the highest pulse energies and build-up times, before the occurrence of optical damage due to pumping. Output energies from 2 to 4 mJ can be produced using a pump intensity of 30 kW cm^{-2} without any deleterious optical damage in the coatings.

Figure 7 shows free-running and Q-switched energies throughout the complete tuning range, when the above coupler is replaced by the grating. The energy discrepancy between the free-running and the Q-switched pulses is determined by a factor of about 2.5, which is consistent with the ratio of the fluorescence decay time to the pump duration. Accounting for a fluorescence decay-time of about 600 µs, this ensures effective energy-storage. As expected, the depletion of the gain due to *ASE* remains negligible inside the stripe.

The value of λ being scanned across the entire tuning bandwidth, we make evidence of significant variations in the corresponding thresholds and in the slope of the laser characteristics. These variations appear to be consistent from a general viewpoint, any decrease in the attainable output energy being related to an increased threshold and a reduced slope. The rather good agreement with predictions from Fig. 3 must be pointed out. Starting from the peak Q-switching efficiency at 1060 nm the laser wavelength is tuned from 1053 to 1065 nm, which results in variations of the output energy from about 0.5 to 2.5 mJ. The build-up time (Fig. 7(b)) then undergoes large variations from about 1 to 3.5 µs.

The shortest build-up time obviously remains related to $\lambda = 1060$ nm, the peak output energy being 2.5 mJ. The discrepancy with the peak former value we measured with the

former coupler in Fig. 6 comes from the penalty due to the amount of additional losses using the grating.

4 Discussion

Let now get back to (1)–(4) to relate the measurement data in Fig. 7 to the theoretical predictions and analyze the tuning process. Even though they do not provide as precise values as those shown in Fig. 3, using the numerical model from *MIRO*, the analytical forms (1)–(4) may be quite useful in the description of representative orders of magnitude. They also help to figure the origin of the wavelength-induced variations in measurable data, such as the energy-transfer laser characteristic and the build-up time (Fig. 7(b)), from the viewpoint of physics. When the pump power is maximum below the limit of optical damage for a selected λ, the measurements of $E_{\text{out}}(\lambda)$ and the evolution of the related laser threshold determine the variation in the effective pumping rate, $k(\lambda)$. We only have to estimate the value of the pump transfer efficiency, denoted as η_{transfer}, to put relevant numbers on the changes in the energy-transfer characteristic $E_{\text{out}}(P_{\text{pump}})$ or $E_{\text{out}}(k)$ versus λ. This is done step by step with the help of separate measurements in the range of values $k \sim 1.05$ to 2. η_{transfer} is the product of a number of terms which include the propagation losses of the pump beam throughout the three cylindrical lenses, the double-pass absorption losses inside the slab and the spatial overlap between the excited area of *LSO* and the modal volume of the cavity. Despite a possible second-order error, we assume the lack of any saturation effect in the absorption process. This will be the main issue yet to be addressed when fitting the experimental results and the predictions. Equations (1), (2) and (4) are derived versus λ, within a given spectral range $\Delta\lambda$, under the following assumptions:

- The derivation versus λ is implemented over a limited spectral range on both sides of 1060 nm, within a maximum spectral range $\Delta\lambda \sim 20$ nm.
- All the wavelength-dependent involved parameters but σ_a are accounted for in the corresponding equations of $E_{\text{out}}(\lambda)$, $T_c(\lambda)$, $G_o(\lambda)$, and $N_{2\text{th}}(\lambda)$. For the sake of simplification, we approximate $\sigma_e(\lambda)$ around 1060 nm with the help of a unique *Lorentzian* of which the line-width equals 8 nm.

This will help to examine the deviations in the prediction of the Q-switched performance, as compared with the modeling results from *MIRO* and with the experimental data. Because $\sigma_a(\lambda)$ undergoes negligible variations with respect to $\sigma_e(\lambda)$, the re-absorption is approximated constant within $\Delta\lambda$. This also helps in simplification. Our actual $\Delta\lambda$ of interest in the fits with predictions extends within the range 1055–1065 nm. Even though the exact value of σ_a does not seem quite easy to determine reading Fig. 1, it can be shown that the plots of parametric calculations using (1), (2) and (4) only lead to representative results when σ_a remains comprised within a certain range of values, $\Delta\sigma_a = [\sigma_{a\_\min} - \sigma_{a\_\max}]$. Outside of $\Delta\sigma_a$, the variations of k do not match the experimental values to be experienced across the whole attainable tuning range in the Q-switched mode of operation. $\Delta\sigma_a = [5 \times 10^{-24}\ \text{cm}^2, 5 \times 10^{-23}\ \text{cm}^2]$ then determines the proper conditions. Furthermore, varying σ_a across $\Delta\sigma_a$ and using (1) to estimate $E_{\text{out}}(\lambda)$ throughout the whole $\Delta\lambda$, it can be shown that some misappreciation of the exact σ_a does not lead to uncertainties in excess of 20%. This way we determined the suitable conditions to make the simple expressions (1)–(4) be consistent with modeling results from *MIRO*, from 1052–1055 to 1065–1070 nm, while preserving less than 10% discrepancy between the possible two calculating procedures. The former wavelengths match the effective $\Delta\lambda$ of interest in the fits with our experimental results.

Let us then illustrate the effectiveness of the analytical model above to figure the optical performance of the design in Fig. 4 and the wavelength-dependence of the related energy-transfer characteristics, as shown in Fig. 6(b). The laser operation is supposed starting at $\lambda = 1060$ nm, in the middle range of the attainable pump intensities to describe the energy-transfer characteristic. Provided $P_{\text{pump}} = 400$ W at the location of the top plane of the slab, (1)–(4) lead to the following set of numbers:

- Regarding the pump efficiency for a gain-stripe of which the top dimensions have been adjusted around $\sim 1.5 \times 3.5\ \text{mm}^2$ under the actual focusing conditions, i.e., a power pump density of $\sim 8\ \text{kW/cm}^2$, we are able to generate a mean inversion density $\sim 0.5 \times 10^{20}\ \text{cm}^{-3}$ and a small-signal gain $G_o \sim 1.16$ at the triggering time of the *Pockels* cell. These values correspond to a doping level $N_{\text{tot}} \sim 10^{21}\ \text{cm}^{-3}$ in the crystal, together with pump storage and absorption efficiencies $\eta_{\text{storage}} \sim 50\%$ and $\eta_{\text{absorption}} = 80\%$, for $T_{\text{pump}} = 1$ ms.
- Regarding the Q-switching performance at $\lambda = 1060$ nm, with $\sigma_e \sim 8 \times 10^{-21}\ \text{cm}^2$, the inversion threshold to be considered is $\sim 6.5 \times 10^{19}\ \text{cm}^{-3}$. We find $k \sim 2.5$. This implies a small-signal gain $G_{o(1060\ \text{nm})} \sim 1.3$, given a cavity of which the total optical losses and length are $\gamma_{\text{tot}} \sim 12\%$ and $L = 15$ cm. We also have to account for a rather poor internal energy-transfer from the viewpoint of elevated losses, on the order of 40%, due to the spatial overlap between the modal volume of the cavity and the gain volume. Considering the amount of initiating noise due to the contributing energy-density of *ASE*, the value of which is $F_{\text{ASE}} \sim 3 \times 10^{-10}\ \text{J cm}^{-2}$ over the actual spectral bandwidth, (1)–(4) lead to $E_{\text{out}(1060\ \text{nm})} \sim 5$ mJ and $T_{c(1060\ \text{nm})} \sim 400$ ns.

– Regarding the tuning performance within the range $\lambda =$ 1056–1064 nm, for similar pump conditions, (1), (2) and (3) lead to a range of effective $k = 1.35$ to 2.2 depending on the value of σ_a. The former values of k, which are obtained for σ_a contained within the range $\Delta\sigma_a$ specified above, correspond to output energies E_{out} ranging from 1 to 4.5 mJ and values of T_c ranging from 1.3 to 3.5 µs.

All these numbers provide useful orders of magnitude in the understanding of the results and of the limitations of our actual design, in relationship with the spectroscopic data of *LSO*. They give the proof that the predictions, either using (1)–(4) or *MIRO*, are consistent with the experimental results. A good agreement is found with the Fig. 6(b), in the situation of the 1.5×2.5 mm^2 gain-stripe:

$$\frac{\partial E}{\partial k} \approx +1.1 \text{ mJ/unit} \quad \text{and} \quad \frac{\partial T_c}{\partial F_{\text{ASE}}} = -3.10^5 \text{ µs cm/J}.$$

On the other hand, they are consistent with the data in Fig. 7, from which the actual evolution of T_c and E_{out} can be estimated versus the selected λ, i.e., versus $\sigma_e(\lambda)$. In the example of $\lambda = 1055$ nm, we get the updated set of theoretical values $E_{\text{out(1055 nm)}} = 3.6$ mJ, $T_{c(1055\text{ nm})} = 300$ ns and $G_{o(1055\text{ nm})} \approx 1.2$. The maximum tuning range, for a given set of the absorbed pump power and optical losses, is limited by the increase of the transparency threshold in the crystal and by the related decrease in the small-signal gain, according to (3). Then (1)–(4) can be considered as an efficient tool for optimizing the pump design.

5 Conclusions and prospects for broadband regenerative amplification

The Q-switched mode of operation of a side-pumped slab of Yb^{3+}:LSO has been shown to enable the generation of pulse energies up to 4 mJ near the peak emission wavelength at 1060 nm, or in the range 1–2.5 mJ throughout a spectral range in excess of 10 nm. Increasing peak pump intensities (20–30 kW cm^{-2}) and gain-stripe length (2.5 to 3 mm), taking into account the limitations imposed by optical damage in standard coatings, wavelength-tuning has been demonstrated from 1055 to 1065 nm, in combination with actual values of the small-signal gain large enough to compensate for ~10% optical losses. Such a performance must be underlined in relationship with the very low emission cross-sections of the material. Furthermore, it needs to be related to fairly consistent modeling predictions, as evidenced by the good agreement between the theoretical and the experimental results. The consistency of both orders of magnitude was verified at small-signal gains in the range 1.1 to 1.3, as well from the viewpoint of the output energy as from the tuning features.

The numbers above then give the proof of the capability of Yb^{3+}:LSO to be used at 1053–1056 nm, the range of wavelengths of interest for *ICF*, for broadband regenerative amplification by means of *CPA*. This will enable the amplification of chirped pulses, within a gain bandwidth in excess of 10 nm, up to a few millijoule energies, with input–output net gains on the order of some 10^4 to 10^6. However, the jump from tunable Q-switching to forthcoming broadband regenerative amplification involves additional work in the following directions:

– The selection of a material at 15% doping level, rather than 10%, to optimize the spatial overlap between the pumped volume and the mode volume of the cavity. The thickness of the slab should be reduced down to 1.2 mm, still preserving the same pump coupling efficiency and gain non-uniformity throughout the amplifying cross-section.
– A longer gain-stripe in order to raise the small-signal gain from $G_o = 1.2$ to 1.4, the peak attainable value in our actual configuration, by juxtaposing a second stack along the first one. This will help to increase the value of k above 3–4 and reduce the build-up times down to 100–200 ns in a standard cavity. The second stack might be imaged into the slab, using the same set of large-aperture cylindrical lenses, to increase the amplifying length from 2.5 mm, the suitable value in the configuration of our paper, up to 5 mm. The implementation of higher pump powers can be managed easily, preserving up to 30 kW cm^{-2} pump intensities without any optical damage.
– The compensation of gain narrowing effects [22], using spectral equalizing techniques to help preserve the most of the spectral bandwidth. As this can be seen in the range of wavelengths located between 1050 and 1065 nm in Fig. 1, due to the slowly varying envelope of $\sigma_e(\lambda)$ in the area, this should be rather easy using volume *Bragg* gratings or adjustable *Lyot* filters.
– The management and the compensation of thermal lens effects, so that the use of a slab may be efficient in the presence of a long optical path. This is a critical issue for regenerative cavities dedicated to the amplification of nanosecond-*FWHM* pulses, with a high beam quality.

The experimental demonstration of a complete *CPA* using of Yb^{3+}:LSO will require the addition of a second diode-stack. This will help to benefit from a longer gain-stripe with a uniform pump density ~20 J cm^{-2}, and enable efficient regenerative amplification around 1060 nm despite the presence of plus or minus large amounts of optical losses in the cavity. Broadband amplification using direct diode-pumping by means of Yb^{3+}:LSO then looks an attractive option in the range of *ICF* wavelengths, to be compared with the technologies based on the use of cascades lasers like *OPCPA* or titanium–sapphire.

Acknowledgements This work was sponsored by Laser funding programs in *CEA/DAM* and *LULI*, within the framework of prospective *R&D* dedicated to the development of future lasers for the *Inertial Confinement Fusion*. The opinions and interpretations are those of the authors and may not be necessarily endorsed by the external commissions.

References

1. E. Hugonnot, G. Deschaseaux, O. Hartmann, H. Coïc, Design of PETAL multi petawatt high-energy laser front end based on optical parametric chirped pulse amplification. Appl. Opt. **46**(33), 8181–8187 (2007)
2. J. Nees, S. Biswal, F. Druon, J. Faure, M. Nantel, G. Mourou, A. Nishimura, H. Takuma, J. Itatani, J.C. Chanteloup, C. Hönninger, Ensuring compactness, reliability and scalability for the next generation of high-field lasers. IEEE J. Sel. Top. Quantum Electron. **4**(2), 376–384 (1998)
3. M. Jacquemet, C. Jacquemet, N. Janel, F. Druon, F. Balembois, P. Georges, J. Petit, B. Viana, D. Vivien, B. Ferrand, Efficient laser action of Yb:LSO and Yb:YSO oxyorthosilicates crystals under high-power diode-pumping. Appl. Phys. B **80**, 171–176 (2005)
4. L. Zheng, G. Zhao, C. Yan, X. Xu, L. Su, Y. Dong, J. Xu, Raman spectroscopic investigation of pure and ytterbium-doped rare earth silicate crystals. J. Raman Spectrosc. **38**, 1421–1428 (2007)
5. L. Zheng, G. Zhao, C. Yan, G. Yao, X. Xu, L. Su, J. Xu, Growth and spectroscopic characteristics of Yb:LPS single crystal. J. Cryst. Growth **304**, 441–447 (2007)
6. G. Bourdet, Comparison of pulse amplification performances in longitudinally pumped Ytterbium doped materials. Opt. Commun. **200**(1–6), 331–342 (2001)
7. J. Du, X. Liang, Y. Xu, R. Li, C. Yan, G. Zhao, L. Su, J. Xu, Z. Xu, Continuous-wave diode-pumped Yb^{3+}:LSO tunable laser. Proc. SPIE **6269**, 627963 (2007)
8. Y. Xu, X. Jiang, J. Du, C. Yan, L. Su, G. Zhao, J. Xu, Efficient tunable diode-pumped CW Yb:LSO laser. Chin. Opt. Lett. **5**, S27–S28 (2007)
9. X. Shi-Xiang, L. Wen-Xue, H. Qiang, Z. Hui, Z. He-Ping, Efficient laser-diode end-pumped passively Q-switched mode-locked Yb:LSO laser based on SESAM. Chin. Phys. Lett. **25**(2), 548–551 (2008)
10. C. Hönninger, I. Johannsen, M. Moser, G. Zhang, A. Giesen, U. Keller, Diode-pumped thin-disk Yb:YAG regenerative amplifier. Appl. Phys. B **65**, 423–426 (1997)
11. C. Hönninger, R. Paschotta, M. Graf, F. Morier-Genoud, G. Zhang, M. Moser, S. Biswal, J. Nees, A. Braun, G. Mourou, I. Johannsen, A. Giesen, W. Seeber, U. Keller, Ultrafast ytterbium-doped bulk lasers and laser amplifiers. Appl. Phys. B **69**, 3–17 (1999)
12. J. Kawanaka, K. Yamakawa, H. Nishioka, K.-I. Ueda, 30 mJ, diode-pumped, chirped-pulse Yb:YLF regenerative amplifier. Opt. Lett. **28**(21), 2121–2123 (2003)
13. H. Liu, S. Biswal, J. Paye, J. Nees, G. Mourou, C. Hönninger, U. Keller, Directly diode-pumped millijoule subpicosecond Yb :glass regenerative amplifier. Opt. Lett. **24**(13), 917–919 (1999)
14. S. Biswal, J. Itatani, J. Nees, G. Mourou, Efficient energy extraction below the saturation fluence in a low-gain low-loss regenerative chirped-pulse amplifier. IEEE J. Sel. Top. Quantum Electron. **4**(2), 421–425 (1998)
15. P. Raybaut, F. Druon, F. Balembois, P. Georges, R. Gaumé, B. Viana, D. Vivien, Directly diode-pumped Yb^{3+}:SrY_4 $(SiO_4)_3O$ regenerative amplifier. Opt. Lett. **28**(22), 2195–2197 (2003)
16. H. Liu, J. Nees, G. Mourou, Directly diode-pumped Yb:KY(WO4)2 regenerative amplifiers. Opt. Lett. **27**(9), 722–724 (2002)
17. J. Du, X. Liang, Y. Xu, R. Li, Z. Xu, Tunable and efficient diode-pumped Yb^{3+}:GYSO laser. Opt. Express **14**(8), 3333 (2006)
18. M. Siebold, M. Hornung, S. Bock, J. Hein, M.C. Kaluza, J. Wemans, R. Uecker, Broad-band regenerative laser amplification in ytterbium-doped calcium fluoride (Yb:CaF2). Appl. Phys. B **89**, 543–547 (2007)
19. F. Thibault, D. Pelenc, F. Druon, Y. Zaouter, M. Jacquemet, P. Georges, Efficient diode-pumped Yb^{3+}:Y_2SiO_5 and Yb^{3+}:Lu_2SiO_5 high-power femtosecond laser operation. Opt. Lett. **31**(10), 1555–1557 (2006)
20. O. Morice, MIRO: Complete modeling and software for pulse amplification and propagation in high-power laser systems. Optim. Eng. **42**(6), 1530–1541 (2003)
21. A. Jolly, E. Artigaut, Theoretical design for the optimization of a material's geometry in diode-pumped high-energy Yb^{3+}:YAG lasers and its experimental validation at 0.5–1 J. Appl. Opt. **43**(32), 6016–6022 (2004)
22. P. Raybaut, F. Balembois, F. Druon, P. Georges, Numerical and experimental study of gain narrowing in Ytterbium-based regenerative amplifiers. IEEE J. Sel. Top. Quantum Electron. **41**(3), 415–425 (2005)